Effective medium optical modelling of indium tin oxide nanocrystal films

Maria Sygletou[1]§, Fabio Marangi[2,3]§, Stefano Varas[4], Alessandro Chiasera[4], Maurizio Canepa[1], Francesco Scotognella[2,3]*, Francesco Bisio[5]*

1 OPTMATLAB Dipartimento di Fisica, Università di Genova, Via Dodecaneso 33, 16146 Genova, Italy

2 Department of Physics, Politecnico di Milano, Piazza L. da Vinci 32, 20133 Milano, Italy

3 Center for Nano Science and Technology@PoliMi, Istituto Italiano di Tecnologia (IIT), Via Giovanni Pascoli, 70/3, 20133, Milan, Italy

4 IFN - CNR CSMFO Lab. & FBK CMM, Trento, Italy

5 CNR-SPIN, Corso Perrone 24, 16152 genova, Italy

§ The authors equally contributed to this work.

E-mail address: francesco.scotognella@polimi.it; francesco.bisio@spin.cnr.it

Abstract

Doped semiconductor nanocrystal-based thin films are widely used for many applications, such as screens, electrochromic windows, light emitting diodes, and solar cells. Herein, we have employed spectroscopic ellipsometry to measure and model the complex dielectric response of indium tin oxide films fabricated by nanocrystal deposition and sintering. The films could be modelled as Bruggemann effective media, allowing to estimate the nanoscale interstitial porosity of the structure. The effective dielectric constant show the possibility of tuning the plasma frequency and the epsilon-near zero condition of the film.

Introduction

Doped-semiconductor thin films that exhibit optical transparency in the visible range are fundamental for applications such as electrodes in screens on portable computers, tablets and smartphones, in electrochromic windows, in light emitting diodes (LEDs), and in solar cells [1–3]. Even if the library of such materials is very broad, including also copper chalcogenides [4,5], the most widely employed materials are doped transition metal oxides, usually referred to as transparent conductive oxides (TCO) [6]. The most popular TCOs are doped zinc oxide [7–10](where doping may be achieved by either one of aluminium, gallium, magnesium, and lithium [11]), fluorine-doped tin oxide (FTO) [12], and indium tin oxide (ITO) [6], the latter two being the most widely used in the current industrial productions [12,13]. Even if a drawback of ITO is represented by indium scarcity, its sibling FTO requires higher temperature processes, increasing fabrication costs, thus limiting its applicability for flexible substrates [12].

ITO thin films are mostly fabricated via sputtering [14–16] and thermal evaporation [9] and such fabrication procedures are well-established. In this respect, a cost reduction in the fabrication of indium tin oxide films is the employment of nanocrystals (NCs) [17,18], since indium tin oxide NCs combine low cost preparation methods with the unique optical and electrical properties of TCO films [19–22]. Moreover, the employment of NC inks to fabricate the films allows fabrication on any surface, either curved or of irregular shape, and superior flexibility with respect to dense and brittle films made by the above-mentioned sputtering and evaporation techniques. The use of NCs also grants the possibility of experimenting with different morphologies, which could be more suitable for specific applications. In fact, NCs can be synthesized in the form of nanospheres, nanorods, nanocubes, nanostars and many other shapes that in turn influence the optical response of the material due to the formation of plasmonic hot-spots [23,24]. This added degree of freedom can be combined with plasmon resonance tunability with doping, opening the way to integration in devices where both morphology and doping play a synergistic role [25].

A reliable determination of the optical properties of NC ITO films, such as the complex refractive index dispersion, is very important to design electrodes for the aforementioned applications. Moreover, the recent research on plasmon-induced hot electron extraction with doped semiconductor NCs [26–28] will benefit from the knowledge of the refractive index dispersion in the near infrared, since this will allow a precise control of the optical properties, in terms of transmission, reflection and absorption, of the material. The visible and near infrared dielectric function dispersion has been determined by transmission, reflection and ellipsometry measurements in sputtered bulk films [29] and in NCs films [18]. However, an effective modelling of the NC-film response in terms of its fundamental constituents, and the implications for plasma frequencies and the respective epsilon-near-zero (ENZ) behaviour is not available.

In this work we investigated the optical properties of NC-based ITO films, focussing the attention on commercially available NCs based on easily scalable fabrication. In order to extrapolate the effective dielectric function, we have relied on the comparison of dense ITO film measurements with the NC-based films. We have employed the Bruggemann effective medium approximation to assess the relative weight of NCs and voids in the film, and extract the related optical response.

Results and Discussion

Dense, bulk-like ITO films (henceforth referred to as "reference ITO") were prepared by RF-sputtering technique. The samples were grown on SiO_2/Si substrates previously outgassed inside the RF-sputtering chamber by means of a 120 °C annealing for 10'. The deposition of the films was performed by sputtering a 15x5 cm^2 ITO target (In_2O_3:SnO_2 90:10 wt%). The residual pressure before growth was about $4.0x10^{-7}$ mbar. During the growth process, the substrates were kept at 30°C. The sputtering was performed with an Ar gas pressure of $5.4x10^{-3}$ mbar with 80 W applied RF power. To monitor the thickness of the layers during the process, a quartz microbalance (Inficon instruments SQM-160) facing the target was employed. The deposition time was 20 minutes corresponding to a nominal thickness of about 180 nm. More details about the fabrication of multilayer structures can be found here [30,31].

Porous, NC-based ITO films (henceforth referred to as "NC film") were prepared by spin-coating. A water dispersion of ITO NCs (20-30 nm) (90:10 In:Sn) by GetNanomaterials was diluted and placed in an ultrasonic bath to favour the separation of bigger NCs aggregates and ensure a more homogeneous dispersion. The dispersion was spin-coated on p-type SiO_2/Si substrates with native oxide, which were previously washed using a standard procedure (10' Water, 10' Acetone, 10' IPA) and treated with oxygen plasma to increase adhesion. Immediately after spin coating, the films were placed in a 1M Formic Acid / Acetonitrile solution bath to remove surface ligands [32]. Subsequently, the samples were annealed at 250 °C for 1h, in a nitrogen atmosphere in order to avoid oxidation of the ITO NCs and preserve the optical properties of the films. Spin-coating deposition leads to a film with a high optical quality, still presenting some voids in between NCs, which are not fully sintered because of the low annealing temperature. The morphology of the films was confirmed by scanning-electron microscopy (SEM), which was also useful to approximately measure the thickness of the samples (≃ 100 nm) to compare it with ellipsometry measurements (Figure 1) .

SEM images have been obtained by using a SEM Tescan Mira 3. To ensure a reasonable conductivity needed for SEM measurements and to highlight the difference between dense sputtered ITO films and porous NC-based films, the samples were deposited on commercial sputtered ITO substrates with the same procedure described above.

UV-Vis-NIR absorption spectra were acquired with a Perkin Elmer Lambda 1050 WB spectrophotometer. The instrument is equipped with deuterium (280–320 nm) and tungsten (320–3300 nm) lamps. The signal is recorded by three detectors working in different spectral regions (photomultiplier [180, 860] nm, InGaAs [860, 1300] nm and PbS [1300, 3300] nm). The measurements were carried out by making use of an integrating sphere in order to take into account scattering contributions and separately record transmission and reflection data. The percentage of absorbed light was calculated as Absorption (%) = 100 - T – R, in which T and R, respectively, stand for the percentage of transmitted and reflected/refracted light. The experimental uncertainties are below 0.5%, meaning that small negative values may appear in near-zero absorption regions. The films for which the data were recorded have been deposited on glass substrates as previously described.

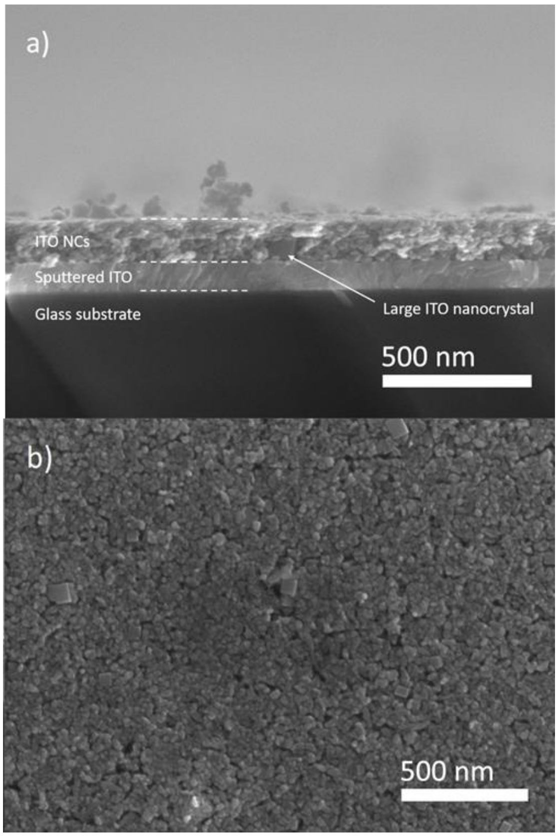

Figure 1. Scanning electron microscopy cross-section (a) and top view (b) of a NCs-based ITO film. A clear difference in morphology is evident with respect to the commercial bulk ITO sputtered film on which the ITO NCs film is deposited.

Variable-angle spectroscopic ellipsometry (SE) measurements were performed by means of a J.A. Woollam V-VASE ellipsometer (190-2500 nm spectral range) and a J.A. Woollam M-2000 ellipsometer (245-1700 nm). SE measures the variation of the state of polarization of light reflected off the samples, quantified by the so-called ellipsometric angles Ψ and Δ, defined according to the equation

$$\boldsymbol{r_p/r_s = tan\,\Psi \cdot e^{i\Delta}}.$$

where, $\boldsymbol{r_{p(s)}}$ are the complex Fresnel reflection coefficients of the system for p (s)-polarized radiation. In Figure 2 we report the ellipsometric spectra of the reference ITO film on SiO_2/Si (open markers). The spectra were measured at 50°, 60° and 70° angle of incidence, in the 245-1700 nm range. The richly-featured spectra carry information about the system morphology and optical response that can be disclosed upon appropriate optical modelling (see next section) [33]. In detail, the peaks in Ψ at around 1 eV and 2.5 eV are due to etaloning across the ITO film, indicative of a thickness in the hundred-nm range. The sharp discontinuities in the Δ spectra are due to the fact that the angle Δ is represented in the -90° to 270° range. The data are here represented as a function of photon energy for graphical-clarity purposes (the VIS-UV features would appear very compressed in the short-wavelength region).

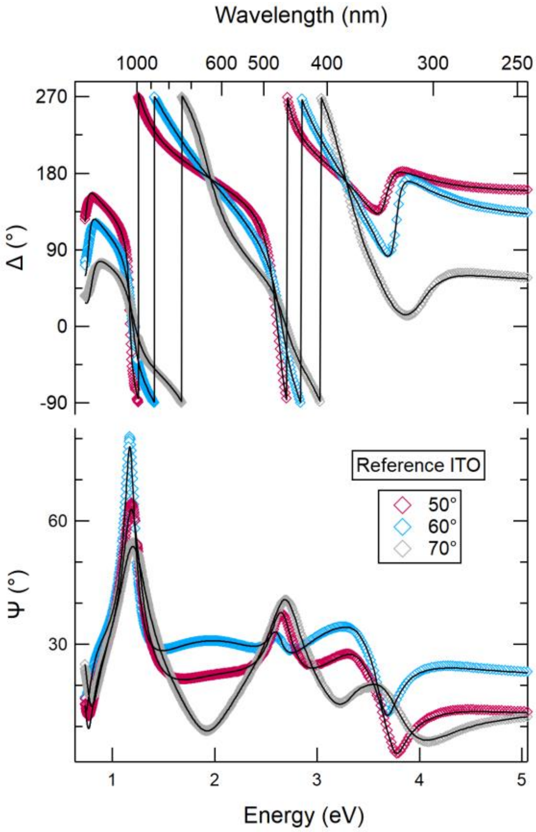

Figure 2. Variable-angle SE spectra of the reference ITO film on SiO2/Si (markers). Best fit to the experimental data (lines).

In Figure 3 we instead report the ellipsometry spectra of a film of ITO NCs, measured at 50° and 60° of incidence (purple and cyan markers, respectively). Here, the spectra are reported as a function of wavelength in order to give more emphasis to the transparency region. We observe that sharp features are present in the UV range, whereas a smoother trend is present all over the VIS-NIR region, with a feature around 1600 nm manifested as a dip in Ψ and a wiggle in Δ.

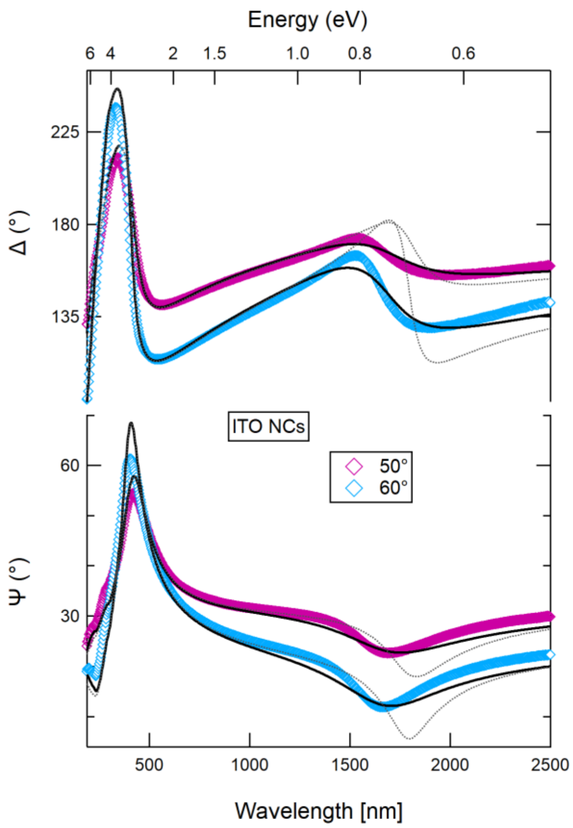

Figure 3. Variable-angle SE spectra of a nanoporous ITO NC film on SiO_2/Si (markers). Best fit of the experimental data obtained allowing a variation of the free-electron contribution to ε (solid black lines) or using the bulk values for ε (dotted lines). See text for details.

Optical modelling & discussion

The optical response of the ITO nanocomposite films can be inferred from their dielectric function. Extracting such a piece of information from the SE data is indeed possible, pending the development of appropriate optical models. The system under scrutiny was accordingly modelled as a stack of *n* dielectric layers, each characterized by its thickness and its complex dielectric function ε_n. The optical response of the system was then calculated assuming Fresnel boundary conditions at the interface between the layers. The optical modelling was performed by means of the WVASE software.

For the reference-ITO film (figure 2), the model included (bottom to top): a semi-infinite Si substrate, a native Si-oxide layer, the ITO film and a roughness layer. The SiO_2/Si substrate was characterized and modelled prior to the ITO deposition by means of the dielectric constants available in the SE software library, in order to limit the number of the free parameters of the fit. The dielectric function of the ITO layer was modelled as the superposition of a Drude component, accounting for the free-carrier contribution, and so-called PSEMI oscillators [34], Kramers-Kronig-consistent functions consisting of piecewise-defined spline polynomials, accounting for the interband transitions. The best fit to the experimental data (black lines in figure 2) was found for an ITO film thickness of 180 nm, a roughness of 3.5 nm, and, most important for us, the complex dielectric function ε_{ITO} reported in figure 4 as the black line (real and imaginary parts). The dielectric function of ITO shows an optical bandgap at (380±10) nm (i.e. 3.25±0.05 eV) and a clear signature of the free-carrier contribution in the NIR, yielding a plasma frequency ω_p at 1800 nm (0.69 eV).

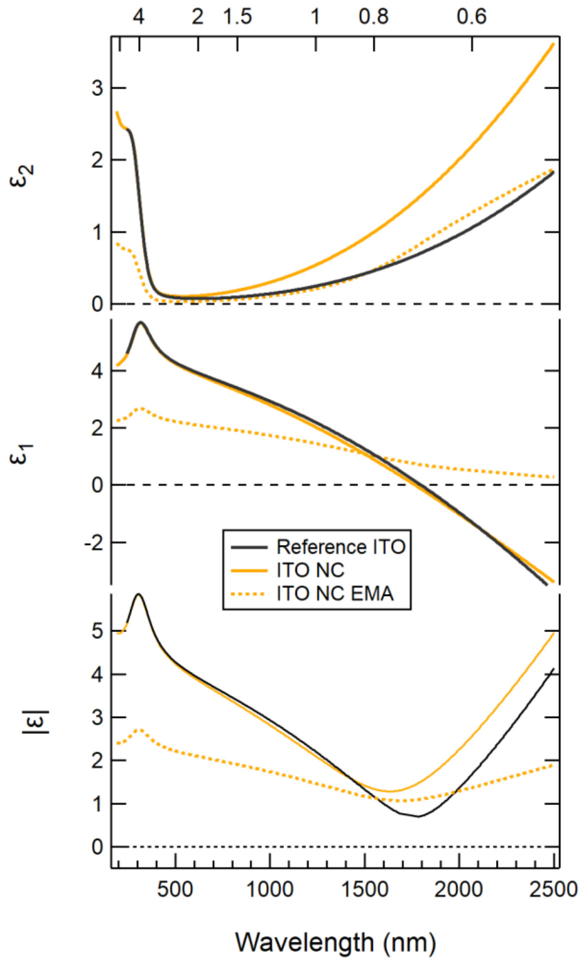

Figure 4. Top panels: real and imaginary parts of dielectric functions of the ITO reference film (black line), of the ITO scaffold in the NC films (solid orange line) and of the whole ITO NC film (dashed orange line). Bottom panel: modulus of the respective dielectric functions.

For the more complex NCs films, the model must account for the peculiar nanomorphology of the NCs layer [35], and for the presence of deviations of the NCs dielectric function with respect to the ITO reference [36]. Accordingly, the model included (bottom to top): a semi-infinite Si substrate with its native oxide layer, and a Bruggeman effective-medium-approximation (BEMA) layer consisting of a mixture of voids (ε=1) and of the ITO scaffold. When fitting the SE data, the film thickness, the fractions of ITO and voids, and the Drude contribution to ε_{ITO} were left as free parameters. The latter is motivated by the fact that the physical constraint of the NC surface typically affects the free-electron mean-free path, leading to enlarged Drude contributions [36]. The interband contribution, though likely affected by the spatial confinement, was assumed unchanged.

The model calculations best matching with the experimental data (continuous black lines in figure 3) were found for a film thickness of (75±5) nm, a void fraction of (50±5)%, and the complex dielectric function of the ITO scaffold reported in Figure 4 as the orange lines. As indeed expected, the dielectric response of the NC scaffold, i.e. the solid fraction of the EMA layer, exhibits an augmented free-electron contribution, arising from a surface-induced increase of the electron-scattering rate compared to the bulk. In order to estimate the influence of this augmented Drude contribution, in figure 3, we also report the Ψ and Δ spectra that were calculated under the constraint of keeping the Drude contribution fixed at its reference-bulk value (dashed grey lines). The fit is clearly worse in these conditions, indicating that the NC- based morphology promotes indeed an increase in electron scattering rate compared to the reference bulk material.

Finally, the *effective* dielectric function of the ITO-NC EMA is reported in Figure 4 as the dashed orange line. Such an effective ε resembles an average between the ITO dielectric function and the one of voids (ε_1=1, ε_2=0). Notably, the UV polarizability and absorption are strongly decreased with respect to the parent material, and the effective plasma frequency is redshifted to above 2.5 µm. The linear absorption, measured independently and reported in figure 5, shows a great affinity with the imaginary part of the EMA dielectric function, supporting further the modelling approach.

The modulus of the dielectric functions of the ITO reference, of the ITO NC “scaffold” and of the EMA are reported in the bottom panel of Figure 4 (black and orange solid lines, and orange dashed line, respectively). It is apparent that the ITO reference has a minimum of its modulus in correspondence of its plasma frequency, which is incidentally the motivation for its exploitation as ENZ material. Interestingly, the dielectric-function modulus of the NC EMA, thanks to a substantially lower ε_1, has a minimum at 1.6 µm which is comparable in magnitude to the bulk ITO film, yet is spectrally decoupled from the plasma frequency, which can be extrapolated around 3 µm. Interestingly, the minimum of $|\boldsymbol{\varepsilon}|$ is manifested in the SE spectra of the NC film as the wiggle in Δ and the corresponding dip in Ψ, making it straightforward to identify this condition from the experimental data.

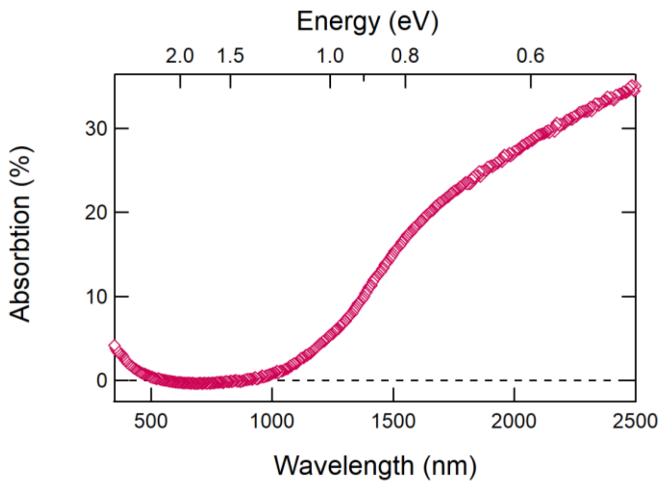

Figure 5. Absorption of the ITO NCline film.

Conclusions

Being one of the most commonly employed transparent conductive oxides, the determination via ellipsometry of the optical properties of a film of commercially available ITO NCs fabricated via spin coating leads to a new level of characterization of the material. The measurements performed, which also resulted in the definition of the epsilon-near-zero (ENZ) range for the material in the form of a NCs thin film, will allow further investigation of nonlinear optical phenomena that enable a great number of applications including spectroscopy [37,38], telecommunications, quantum information technologies and so on [39]. The huge nonlinear optical response with a sub-picosecond time response and the morphology of the material in the form of NCs make it suitable for nanoscale integration with common fabrication technologies [39,40].

In addition, when considering doped semiconductor NCs, it must be taken into account that their plasmonic response strongly depends on their percentage of doping. In fact, the density of free carriers strongly influences the plasma frequency, which shifts to longer wavelengths as the density of carriers decreases [20]. Doped-semiconductor NCs can be easily synthesized with variable percentages of doping, making it possible to tune their plasma frequency, thus their optical response and ENZ range, as required by the intended application [38,39,41]. In addition, the dependence of plasma frequency on carrier concentration has not been investigated in the ENZ regime yet. Thus, the demonstration of a reliable technique for the definition of such a range of frequencies on a number of different materials in the form of NCs can provide a good starting point for further investigation on the subject.

In this work we have successfully employed spectroscopic ellipsometry to determine the complex dielectric function of NC-based ITO films. This will allow the comprehension of such types of porous transparent conductive films. Since ITO is interesting for hot electron extraction in the infrared at the interface with a proper semiconductor, a further study could involve mixed NC films that include ITO and semiconductor NCs.

References

1 R. A. Afre, N. Sharma, M. Sharon and M. Sharon, Transparent Conducting Oxide Films for Various Applications: A Review, *REVIEWS ON ADVANCED MATERIALS SCIENCE*, 2018, **53**, 79–89.
2 X. Ji, J. Song, T. Wu, Y. Tian, B. Han, X. Liu, H. Wang, Y. Gui, Y. Ding and Y. Wang, Fabrication of high-performance F and Al co-doped ZnO transparent conductive films for use in perovskite solar cells, *Solar Energy Materials and Solar Cells*, 2019, **190**, 6–11.
3 T. Gatti, F. Lamberti, R. Mazzaro, I. Kriegel, D. Schlettwein, F. Enrichi, N. Lago, E. Di Maria, G. Meneghesso, A. Vomiero and S. Gross, Opportunities from Doping of Non-Critical Metal Oxides in Last Generation Light-Conversion Devices, *Adv. Energy Mater.*, 2021, **11**, 2101041.
4 I. Grozdanov, C. K. Barlingay and S. K. Dey, Deposition of transparent and electroconductive chalcogenide films at near-room temperatures, *Integrated Ferroelectrics*, 1995, **6**, 205–211.
5 C. Guillén and J. Herrero, Copper oxy-sulfide and copper sulfate thin films as transparent p-type conductive electrodes, *Materials Research Bulletin*, 2018, **101**, 116–122.
6 D. S. Ginley and C. Bright, Transparent Conducting Oxides, *MRS Bulletin*, 2000, **25**, 15–18.
7 J. Rousset, E. Saucedo and D. Lincot, Extrinsic Doping of Electrodeposited Zinc Oxide Films by Chlorine for Transparent Conductive Oxide Applications, *Chem. Mater.*, 2009, **21**, 534–540.

8 X. Jiang, F. L. Wong, M. K. Fung and S. T. Lee, Aluminum-doped zinc oxide films as transparent conductive electrode for organic light-emitting devices, *Appl. Phys. Lett.*, 2003, **83**, 1875–1877.

9 G. Socol, M. Socol, N. Stefan, E. Axente, G. Popescu-Pelin, D. Craciun, L. Duta, C. N. Mihailescu, I. N. Mihailescu, A. Stanculescu, D. Visan, V. Sava, A. C. Galca, C. R. Luculescu and V. Craciun, Pulsed laser deposition of transparent conductive oxide thin films on flexible substrates, *Applied Surface Science*, 2012, **260**, 42–46.

10 M. Sygletou, F. Bisio, S. Benedetti, P. Torelli, A. di Bona, A. Petrov and M. Canepa, Transparent conductive oxide-based architectures for the electrical modulation of the optical response: A spectroscopic ellipsometry study, *Journal of Vacuum Science & Technology B*, 2019, **37**, 061209.

11 A. Alexandrov, M. Zvaigzne, D. Lypenko, I. Nabiev and P. Samokhvalov, Al-, Ga-, Mg-, or Li-doped zinc oxide nanoparticles as electron transport layers for quantum dot light-emitting diodes, *Scientific Reports*, 2020, **10**, 7496.

12 D. Jayathilake and T. Nirmal Peiris, Overview on Transparent Conducting Oxides and State of the Art of Low-cost Doped ZnO Systems, *SF Journal of Material and Chemical Engineering*, 2018, **1**, 7.

13 Y.-H. Tak, K.-B. Kim, H.-G. Park, K.-H. Lee and J.-R. Lee, Criteria for ITO (indium–tin-oxide) thin film as the bottom electrode of an organic light emitting diode, *Thin Solid Films*, 2002, **411**, 12–16.

14 T. Karasawa and Y. Miyata, Electrical and optical properties of indium tin oxide thin films deposited on unheated substrates by d.c. reactive sputtering, *Thin Solid Films*, 1993, **223**, 135–139.

15 M. Kang, I. Kim, M. Chu, S. W. Kim and J.-W. Ryu, Optical Properties of Sputtered Indium-tin-oxide Thin Films, *Journal of the Korean Physical Society*, 2011, **59**, 3280–3283.

16 K. Ellmer and T. Welzel, Reactive magnetron sputtering of transparent conductive oxide thin films: Role of energetic particle (ion) bombardment, *Journal of Materials Research*, 2012, **27**, 765–779.

17 J. Ederth, P. Heszler, A. Hultåker, G. A. Niklasson and C. G. Granqvist, Indium tin oxide films made from nanoparticles: models for the optical and electrical properties, *Thin Solid Films*, 2003, **445**, 199–206.

18 R. J. Mendelsberg, G. Garcia and D. J. Milliron, Extracting reliable electronic properties from transmission spectra of indium tin oxide thin films and nanocrystal films by careful application of the Drude theory, *Journal of Applied Physics*, 2012, **111**, 063515.

19 A. Agrawal, R. W. Johns and D. J. Milliron, Control of Localized Surface Plasmon Resonances in Metal Oxide Nanocrystals, *Annual Review of Materials Research*, 2017, **47**, 1–31.

20 I. Kriegel, F. Scotognella and L. Manna, Plasmonic doped semiconductor nanocrystals: Properties, fabrication, applications and perspectives, *Physics Reports*, 2017, **674**, 1–52.

21 I. Kriegel, M. Ghini, S. Bellani, K. Zhang, A. W. Jansons, B. M. Crockett, K. M. Koskela, E. S. Barnard, E. Penzo, J. E. Hutchison, J. A. Robinson, L. Manna, N. J. Borys and P. J. Schuck, Light-Driven Permanent Charge Separation across a Hybrid Zero-Dimensional/Two-Dimensional Interface, *J. Phys. Chem. C*, 2020, **124**, 8000–8007.

22 G. M. Paternò, C. Iseppon, A. D'Altri, C. Fasanotti, G. Merati, M. Randi, A. Desii, E. A. A. Pogna, D. Viola, G. Cerullo, F. Scotognella and I. Kriegel, Solution processable and optically switchable 1D photonic structures, *Sci Rep*, 2018, **8**, 1–8.

23 J. Reguera, J. Langer, D. J. de Aberasturi and L. M. Liz-Marzán, in *Colloidal Synthesis of Plasmonic Nanometals*, Jenny Stanford Publishing, 2020.

24 T. Sasaki, Y. Endo, M. Nakaya, K. Kanie, A. Nagatomi, K. Tanoue, R. Nakamura and A. Muramatsu, One-step solvothermal synthesis of cubic-shaped ITO nanoparticles precisely

controlled in size and shape and their electrical resistivity, *Journal of Materials Chemistry*, 2010, **20**, 8153–8157.
25 S. Heo, S. H. Cho, C. J. Dahlman, A. Agrawal and D. J. Milliron, Influence of Crystalline and Shape Anisotropy on Electrochromic Modulation in Doped Semiconductor Nanocrystals, *ACS Energy Lett.*, 2020, **5**, 2662–2670.
26 C. Clavero, Plasmon-induced hot-electron generation at nanoparticle/metal-oxide interfaces for photovoltaic and photocatalytic devices, *Nature Photon*, 2014, **8**, 95–103.
27 M. Sakamoto, T. Kawawaki, M. Kimura, T. Yoshinaga, J. J. M. Vequizo, H. Matsunaga, C. S. K. Ranasinghe, A. Yamakata, H. Matsuzaki, A. Furube and T. Teranishi, Clear and transparent nanocrystals for infrared-responsive carrier transfer, *Nat Commun*, 2019, **10**, 1–7.
28 D. Zhou, X. Li, Q. Zhou and H. Zhu, Infrared driven hot electron generation and transfer from non-noble metal plasmonic nanocrystals, *Nat Commun*, 2020, **11**, 2944.
29 Y. Wang, A. C. Overvig, S. Shrestha, R. Zhang, R. Wang, N. Yu and L. D. Negro, Tunability of indium tin oxide materials for mid-infrared plasmonics applications, *Opt. Mater. Express, OME*, 2017, **7**, 2727–2739.
30 O. Sayginer, E. Iacob, S. Varas, A. Szczurek, M. Ferrari, A. Lukowiak, G. C. Righini, O. S. Bursi and A. Chiasera, Design, fabrication and assessment of an optomechanical sensor for pressure and vibration detection using flexible glass multilayers, *Optical Materials*, 2021, **115**, 111023.
31 A. Chiasera, C. Meroni, F. Scotognella, Y. G. Boucher, G. Galzerano, A. Lukowiak, D. Ristic, G. Speranza, S. Valligatla, S. Varas, L. Zur, M. Ivanda, G. C. Righini, S. Taccheo, R. Ramponi and M. Ferrari, Coherent emission from fully Er3+ doped monolithic 1-D dielectric microcavity fabricated by rf-sputtering, *Optical Materials*, 2019, **87**, 107–111.
32 G. Garcia, R. Buonsanti, E. L. Runnerstrom, R. J. Mendelsberg, A. Llordes, A. Anders, T. J. Richardson and D. J. Milliron, Dynamically Modulating the Surface Plasmon Resonance of Doped Semiconductor Nanocrystals, *Nano Lett.*, 2011, **11**, 4415–4420.
33 M. Canepa, in *Surface Science Techniques*, eds. G. Bracco and B. Holst, Springer, Berlin, Heidelberg, 2013, pp. 99–135.
34 United States Patent, 5796983, 1998.
35 C. Toccafondi, S. Uttiya, O. Cavalleri, G. Gemme, E. Barborini, F. Bisio and M. Canepa, Optical properties of nanogranular and highly porous TiO2thin films, *J. Phys. D: Appl. Phys.*, 2014, **47**, 485301.
36 F. Bisio, M. Palombo, M. Prato, O. Cavalleri, E. Barborini, S. Vinati, M. Franchi, L. Mattera and M. Canepa, Optical properties of cluster-assembled nanoporous gold films, *Phys. Rev. B*, 2009, **80**, 205428.
37 L. Rodríguez-Suné, M. Scalora, A. S. Johnson, C. Cojocaru, N. Akozbek, Z. J. Coppens, D. Perez-Salinas, S. Wall and J. Trull, Study of second and third harmonic generation from an indium tin oxide nanolayer: Influence of nonlocal effects and hot electrons, *APL Photonics*, 2020, **5**, 010801.
38 J. Yoon, M. Zhou, M. A. Badsha, T. Y. Kim, Y. C. Jun and C. K. Hwangbo, Broadband Epsilon-Near-Zero Perfect Absorption in the Near-Infrared, *Sci Rep*, 2015, **5**, 12788.
39 O. Reshef, I. De Leon, M. Z. Alam and R. W. Boyd, Nonlinear optical effects in epsilon-near-zero media, *Nat Rev Mater*, 2019, **4**, 535–551.
40 F. Marangi, M. Lombardo, A. Villa and F. Scotognella, (INVITED) New Strategies for Solar Cells Beyond the Visible Spectral Range, *Optical Materials: X*, 2021, **11**, 100083.
41 L. Caspani, R. P. M. Kaipurath, M. Clerici, M. Ferrera, T. Roger, J. Kim, N. Kinsey, M. Pietrzyk, A. Di Falco, V. M. Shalaev, A. Boltasseva and D. Faccio, Enhanced Nonlinear Refractive Index in $\ensuremath{\epsilon}$-Near-Zero Materials, *Phys. Rev. Lett.*, 2016, **116**, 233901.